CFD SIMULATION OF A SOLVENT EXTRACTION PUMP MIXER UNIT: EVALUATING LARGE EDDY SIMULATION AND RANS BASED MODELS.

Mandar TABIB*, **Graeme LANE, William YANG and M Philip SCHWARZ**

CSIRO Process Science and Engineering, Clayton, Victoria 3169, AUSTRALIA

*Corresponding author, E-mail address: mandar.tabib@csiro.au

ABSTRACT

Mixer-settler equipment is widely used for solvent extraction (SX) operations. The pump mixer is the heart of an SX process. Any improvement in understanding of hydrodynamics and flow instabilities within a SX pump mixer unit would enable effective design of the mixer-settler equipment. In this direction, the present work investigates the predictive performance of the Large Eddy Simulation (LES) model vis-à-vis the PIV experimental results and RANS based model. Comparisons have been made initially for single phase operation of a Mixer unit, and then for the multiphase operation. The ANSYS/CFX modelling package has been used to set-up a transient three-dimensional CFD model using the sliding mesh approach for impeller motion and Eulerian-Eulerian approach for multi-phase flows. The present paper compares the flow patterns predicted by the LES model and compares them to RANS model prediction and PIV data. The prediction of flow structures and turbulence intensities will pave the way for determination of droplet size and mass transfer rates, which are required in designing these systems.

NOMENCLATURE

C_D drag force coefficient, dimensionless
Cs smagorinsky Constant, dimensionless
C_μ constant in k-ε model, dimensionless
d_B bubble diameter, m
G generation term, kg m^{-1} s^{-2}
k turbulent kinetic energy per unit mass, m^2 s^{-2}
$\mathbf{M_I}$ total interfacial force between two phases, N m^{-3}
P pressure, N m^{-2}
S strain rate, s^{-1}.
t time, s
$\mathbf{u}$ velocity vector, ms^{-1}
u' fluctuating velocity, ms^{-1}
$\mathbf{u}_{inst}$ instantaneous velocity, ms^{-1}
$\mathbf{u}_{sgs}$ sub-grid scale velocity, ms^{-1}
α fractional phase hold-up, dimensionless
ε turbulent energy dissipation rate per unit mass, m^{2}s^{-3}
μ_{eff} effective viscosity, Pa s
τ_k shear stress of phase k, Pa
Δ Grid size, m
Subscript
 R   Resolved
 S   Sub-grid scale
 j   phase
 a   Continuose Aqueous phase
 o   Dispersed Organic Phase

INTRODUCTION

Solvent extraction based hydrometallurgy processes are mainly used in copper, nickel, uranium and cobalt industries and are implemented through frequent use of the Mixer-Settler equipment. A typical mixer settler set-up (as shown in Fig. 1) involves a solvent extraction pump mixer, comprising of a mixing impeller, a false bottom for inlet of fluids and a weir at the top for discharge. The impeller on rotation creates a pressure drop or head that generates the flow, and creates a high shear region for droplet formation and break-up. The main design objective in the mixer section involves achieving a sufficiently small droplet size for mass transfer to take place, without generating a population of fine droplets that will be difficult to separate in the settler. One way of achieving this is through a proper understanding of hydrodynamics and turbulent conditions within the mixer unit but this requires an advanced turbulence modelling approach. Recently, the Large Eddy Simulation (LES) turbulence model has shown significant promise in unearthing flow details in stirred tanks (Derksen et al., 2007; Murthy et al., 2008), in gas-liquid multiphase systems, (Deen et al., 2001; Dhotre et al., 2008; Niceno et al., 2008; Tabib et al., 2009) and in liquid-solid particle systems involving stirred vessel (Derksen et al., 2006; Hartmann et al., 2006; Lane G., 2006). To the author's knowledge, the use of LES for predicting flow phenomena in a multiphase liquid-liquid stirred tank system like an SX-Pump Mixer hasn't been attempted. This work attempts to ascertain the predictive capability of the ANSYS/CFX-12 LES models vis-à-vis RANS and an experimental dataset. Generally, for accuracy in multiphase systems, the Euler-Lagrangian LES approach is recommended, but it is computationally impossible to apply this when the dispersed phase volume fractions/particle density is high. Hence, we apply the Euler-Euler LES approach for our case. In the following sections, the model has been mathematically described and its implementations discussed. This is followed by results and conclusion.
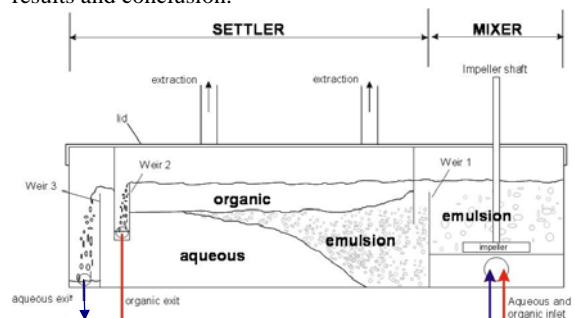

Figure 1: Schematic diagram of geometry.

MODEL DESCRIPTION

The numerical simulations presented are based on both a single phase and multiphase model. For space reasons, the multiphase model is described, which is a two-fluid model based on the Euler-Euler approach. Here, each fluid (or phase) is treated as a continuum in any size of domain under consideration. The phases share this domain and interpenetrate as they move within it. The Eulerian modelling framework is based on ensemble-averaged mass and momentum transport equations for each of these phases. These transport equations without mass transfer can be written as:

Continuity equation

$$\frac{\partial}{\partial t}\left(\rho_j \alpha_j\right) + \nabla \cdot \left(\rho_j \alpha_j \mathbf{u}_j\right) = 0 \qquad (1)$$

Momentum transfer equations

$$\frac{\partial}{\partial t}\left(\rho_j \alpha_j \mathbf{u}_j\right) + \nabla \cdot \left(\rho_j \alpha_j \mathbf{u}_j \mathbf{u}_j\right) = -\nabla \cdot \left(\alpha_j \tau_j\right)$$
$$- \alpha_j \nabla P + \alpha_j \rho_j g + M_{F,j} \qquad (2)$$

In this work, the phases are continuous aqueous phase ($j=a$) and dispersed organic phase ($j=o$). The terms on the right hand side of eq. (2) are respectively representing the stress, the pressure gradient, gravity and the ensemble averaged momentum exchange between the phases, due to interface forces. The pressure is shared by both the phases. The stress term of phase k is described as follows:

$$\tau_j = -\mu_{eff,j}\left(\nabla \mathbf{u}_j + \left(\nabla \mathbf{u}_j\right)^T - \frac{2}{3}I\left(\nabla.\mathbf{u}_j\right)\right) \qquad (3)$$

where, $\mu_{eff,j}$ is the effective viscosity. The effective viscosity of the continuous aqueous phase is composed of two contributions: the molecular viscosity and the turbulent viscosity.

$$\mu_{eff,a} = \mu_{l,a} + \mu_{t,a} \qquad (4)$$

The aqueous phase turbulent eddy viscosity ($\mu_{t,a}$) is formulated based upon the turbulence model used (k-ε turbulence model or Large Eddy Simulation Turbulence Model). The calculation of the effective organic dispersed phase viscosity is based on the effective aqueous phase viscosity as follows:

$$\mu_{eff,o} = \left(\frac{\rho_a}{\rho_o}\right)\mu_{eff,a} \qquad (5)$$

The total interfacial force acting between the two phases may arise from several independent physical effects:

$$M_{I,a} = -M_{I,o} = M_{D,a} + M_{L,a} + M_{VM,a} + M_{TD,a} \qquad (6)$$

The forces indicated above represent the interphase drag force, lift force, virtual mass force and turbulent dispersion force respectively. For liquid-liquid flow, the contributions of lift force, virtual mass force and turbulent dispersion force can be neglected and only drag force needs to be considered. The origin of the drag force is due to the resistance experienced by a body moving in the liquid. Viscous stress creates skin drag and pressure distribution around the moving body creates form drag. The later mechanism is due to inertia and becomes significant as the particle Reynolds number becomes larger. The interphase momentum transfer due to drag force is given by:

$$\mathbf{F}_{drag,a} = -\mathbf{F}_{drag,o} = -\frac{3}{4}\alpha_o \rho_1 \frac{C_D}{d}\left|\mathbf{U}_o - \mathbf{U}_a\right|\left(\mathbf{U}_o - \mathbf{U}_a\right) \qquad (7)$$

where, C_D is the drag coefficient taking into account the character of the flow around the droplet, and d_B is the droplet diameter. The drag coefficient was determined through the empirical correlations of Ishii and Zuber (1979), which allow for an increase in drag (and reduced rise velocity) due to multiple droplet interactions, as a function of the dispersed organic phase volume fraction. For the viscous regime, the drag coefficient was determined according to:

$$C_{Da} = \frac{24}{\text{Re}}\left(1 + 0.1\text{Re}^{0.75}\right) \qquad (8)$$

where the Reynolds number, Re, is modified to allow for the dispersed phase volume fraction and is given by:

$$\text{Re} = \frac{\rho_a \left|\mathbf{U}_o - \mathbf{U}_a\right| d}{\mu_a}\left(1 - \alpha_o\right) \qquad (9)$$

For the distorted regime,

$$C_{D,o} = \frac{2}{3}d\sqrt{\frac{(\rho_a - \rho_o)g}{\sigma}}\left(1 - \alpha_o\right)^{-0.5} \qquad (10)$$

The drag coefficient was chosen according to:

$$C_D = \max\left(C_{D,a}, C_{D,o}\right). \qquad (11)$$

k-ε turbulence model

When the k-ε model is used, the velocities (**u**) in continuity equations and momentum equations (eq.1-2) represent the time averaged velocities. The turbulent eddy viscosity is formulated as follow

$$\mu_{t,a} = \rho_a C_\mu \frac{k^2}{\varepsilon} \qquad (12)$$

The turbulent kinetic energy (k) and its energy dissipation rate (ε) are calculated from their governing equations:

$$\frac{\partial}{\partial t}\left(\rho_a \alpha_a k\right) + \nabla \cdot \left(\rho_a \alpha_a \mathbf{u}_a k\right) = -\nabla \cdot \left(\alpha_a \frac{\mu_{eff,a}}{\sigma_k}\nabla k\right)$$
$$+ \alpha_a \left(G - \rho_a \varepsilon\right) \qquad (13)$$

$$\frac{\partial}{\partial t}\left(\rho_a \alpha_a \varepsilon\right) + \nabla \cdot \left(\rho_a \alpha_a \mathbf{u}_a \varepsilon\right) = -\nabla \cdot \left(\alpha_a \frac{\mu_{eff,a}}{\sigma_\varepsilon}\nabla \varepsilon\right)$$
$$+ \alpha_a \frac{\varepsilon}{k}\left(C_{\varepsilon 1}G - C_{\varepsilon 2}\rho_a \varepsilon\right) \qquad (14)$$

The model constants are C_μ =0.09; σ_k=1.00; σ_ε=1.00; $C_{\varepsilon 1}$=1.44, $C_{\varepsilon 2}$=1.92. The term G in above equation is the production of turbulent kinetic energy and described by:

$$G = \tau_a : \nabla \mathbf{u}_a \qquad (15)$$

Large Eddy Simulation Turbulence Model

Equations for LES are derived by applying a filtering operation to the Navier-Stokes equations. The filtered equations are used to compute the dynamics of the large-scale structures, while the effect of the small scale turbulence is modeled using a Sub Grid Scale model. Thus, the entire flow field is decomposed into a large-scale or resolved component and a small-scale or subgrid-scale component. In this work, the Smagorinsky model (Smagorinsky, 1963), Dynamic Smagorinsky Model (Germano et al., 1992; Lily, 1993) has been used. In case of LES, the velocities (**u**) in continuity equations and momentum equations (eq.1-2) represent the resolved velocities or grid scale velocities.

$$u = u_{inst} - u_{SGS} \qquad (16)$$

The turbulent eddy viscosity is formulated depending upon the LES model selected:

Smagorinsky Constant

$$\mu_{T,a} = \rho_a (C_s \Delta)^2 |S|^2 \qquad (17)$$

Where, *Cs* is the Smagorinsky constant, *S* is the strain rate and Δ is the filter width $= (\Delta_i \Delta_j \Delta_k)^{1/3}$. The constant *C*s is different for different flows. In the literature for single-phase flow, the constant is found to vary in the range from *C*s = 0.065 to *C*s = 0.25 (Moin et al., 1982).

Dynamic Smagorinsky Model

The uncertainty in specifying the constant *C*s in Smagorinsky model led to the development of dynamic sub-grid model (Germano et al., 1991; Lilly et al., 1992) in which the constant *C*s is computed. The main idea here is to introduce a filter $\{\Delta\}$, with larger width than the original one, i.e. $\{\Delta\} > \Delta$. This filter is applied to the filtered Navier–Stokes equations (the NS equations are filtered twice), yielding the value of *C*s derived from:

$$C_s = \frac{1}{2} \frac{L_{ij} M_{ij}}{M_{ij} M_{ij}} \qquad (18)$$

where,

$$L_{ij} = \{\overline{u_i u_j}\} - \{\overline{u_i}\}\{\overline{u_j}\} \qquad (19)$$

and,

$$M_{ij} = \left[\{\Delta\}^2 \{\overline{|S|}\}\{\overline{S_{ij}}\} - \{\Delta\}^2 \{\overline{|S|S_{ij}}\} \right] \qquad (20)$$

$$\mu_{T,a} = \rho_a (C_s \Delta)^2 |S|^2 \qquad (21)$$

The $\{\ \}$ indicates a second filter, usually called the test filter, which is twice the mesh size in the present study, has been applied to the velocity field.

Model Application

a) Geometry

The mixer unit comprises of a square mixer box (of dimensions 450mmx450mmx450mm) equipped with a Lightnin R320 pump-mixer (of diameter 230 mm and positioned about 5 mm above the false bottom). The mixer has been modelled with an impeller speed of 200 rpm (tip speed of 2.4 m/s). In this work, only the pump-mixer region has been simulated. There is a separate inlet section for the organic and aqueous phases located in the bottom section below, where they flow in at a rate of 15 l/min each. The outlet from the mixer box is in the form of an overflow via a weir to a rectangular settler (of dimensions 1410mmx450mm).

#### b) Resolution Issues while applying LES

The accuracy of LES simulations depends upon the following issues.

i. Grid size

For accurate LES results, the modelled SGS stress should account for a negligible fraction of the total stress. In other words, the grid should be sufficiently fine so that smaller, isotropic eddies are modelled. Baggett et al. (1997) suggested that SGS stress becomes isotropic when filter width is a fraction of turbulent dissipation length scale (preferably, 0.1). This has been used in this work as the criteria for obtaining an appropriate grid size. The turbulent dissipation length scale has been obtained from k and ε values of the k-ε model. The volumetric average of ratio $(Vol)^{1/3} / (k_a^{1.5}/\varepsilon_a)$ is around 0.6, and a contour plot of this on horizontal plane can be seen in Fig. 2. Further, the smallest Kolmogorov length scale $\left(v^3/\varepsilon\right)$ for flow generated by the present impeller is around 60μm. In the bulk of the tank region and false bottom region, the grid size is around 100 times the Kolmogorov length scale, which can be considered as reasonable (as the grid size falls in the inertial range). Thus, the grid though a bit coarse, can be regarded as suitable for moderately resolved LES simulations. Hexahedral elements were used with the computational mesh consisting of 587 000 cells with relatively fine mesh near impeller to better resolve the velocity fields (as seen in Fig. 3). In pump mixers, the turbulent structures are generated by large and rotating geometrical features and flow curvature. Hence, the near wall spacing criteria is relaxed with use of appropriate wall functions.
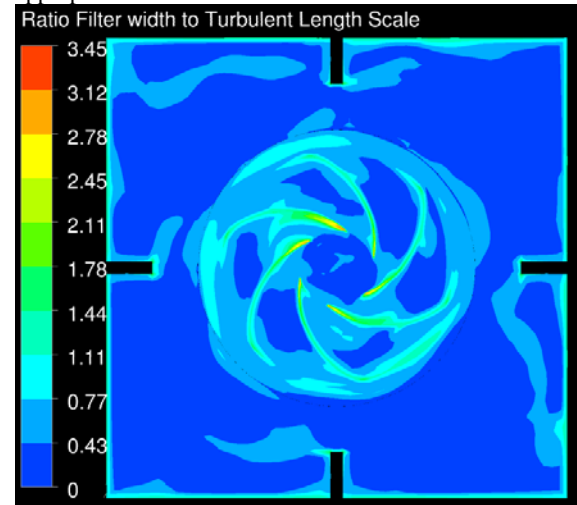
Figure 2: A contour of ratio of Grid length to Turbulent length that measures sufficiency of grid size.
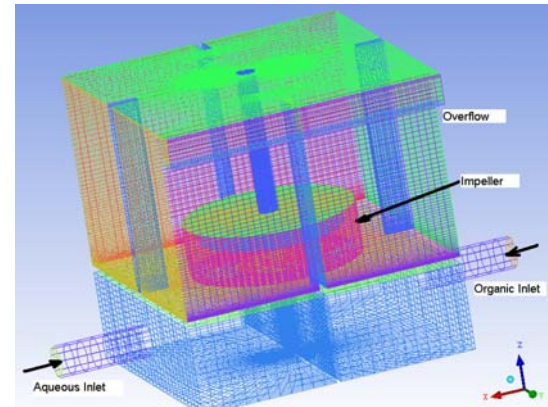
Figure 3. Typical Grid used in this study

ii. Modelled SGS Turbulent Kinetic energy

Pope (2000) suggested that the ratio of resolved turbulent kinetic energy to the total turbulent kinetic energy $\left(k_R \big/ \left(k_R + k_{SGS}\right)\right)$ be used as a measure to analyse the adequacy of the fluid flow being resolved by LES. For well-resolved flow, the ratio is greater than 80%. In this work the ratio is above 70% when averaged over the tank, and in regions with higher turbulence near impeller and in bulk, the ratio is greater than 80%. Fig. 4 represents the contour of this ratio. The results from this LES run can be considered to moderately resolved and acceptable for analysis.
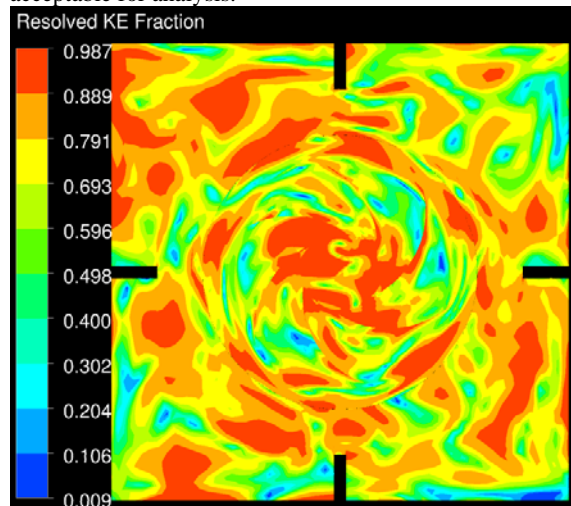
Figure 4: Contour plot of ratio of Resolved KE to Total KE

iii. Modelling Details

The ANSYS/CFX modelling package has been used to set-up a transient three-dimensional CFD model using the sliding mesh approach for impeller motion and Euler-Euler approach for multi-phase flows. For single phase, the aqueous phase inlet velocity is 30 l/min. For multi-phase, both aqueous phase (1000 kg/m^3 density, 1 cp viscocity) and organic phase (930 kg/m^3 density, 3 cp viscocity) enter through separate inlets at 15 l/min. The through-flow rate was determined based on a target residence time of 2 minutes in the mixer. The pump-mixer comprises of a R320 impeller revolving at 200 rpm. For $k - \varepsilon$ model, the high-resolution scheme has been used and for LES, the central difference scheme has been used for spatial discretization of the advection terms. The second-order implicit scheme has been used for time discretization in both the cases. The LES run has been initialized with a perturbed RANS transient solution run to achieve steady flow (around 20 impeller rotations). For $k - \varepsilon$ runs, the time-step has been the time taken by impeller to revolve by 15° (around 0.01 s) and for LES, it's around 8e-4 sec. The selected time-step ensures proper convergence and capture of transient flow structures. The simulations were performed for a time-span of around 10 sec, which corresponds to around 33 revolutions of impeller. For multiphase simultion, the average droplet diameter was taken as 0.6 mm, based on the results from experimental photographic techniques (Fig. 5). For measurement purposes, a miniature low-power light source inside the mixer was used in combination with external additional external lighting in order to improve the image contrast. It was ensured that the there is no obstruction to the flow through measurement set-up.
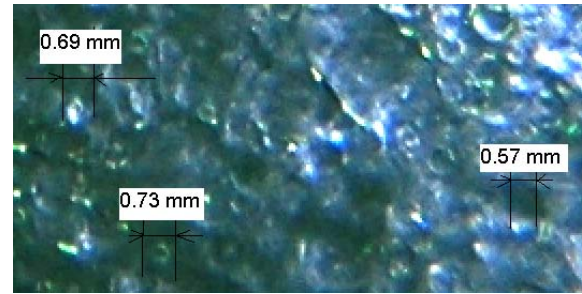

Figure 5: Droplet size measurements in the mixer – geometrical centre of the mixer wall.

RESULTS

Particle Image Velocimetry studies have been carried out at CSIRO Minerals for a single phase Pump Mixer unit operation. The prediction of axial average velocity profile has been used to compare different models (RANS, LES-Smagorinsky, LES-Dynamic). The LES study has been extended to Multiphase after validation in single phase.

Results for Single Phase Mixer

Time averaged Profile

Fig. 6 (A-D) shows the qualitative predictions of velocity vectors as obtained by various models as compared to the PIV Experimental Data at a plane located at x=-0.112. In PIV snapshot (Fig. 6A), at the right side of impeller, the recirculating flow doesn't reach the top right side wall. The Smagroinsky LES Model (Fig. 6B) is closer to the flow pattern given by the PIV experiment.
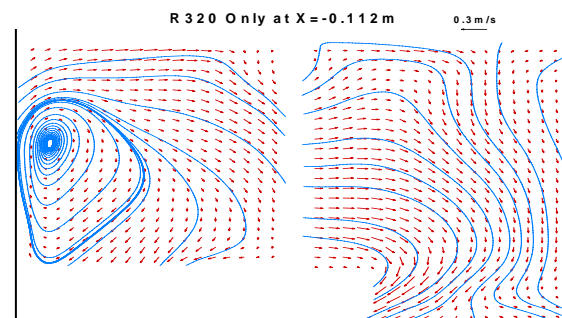

Figure 6A. PIV Experimental Snapshot of time averaged profile at x=-0.112 location.
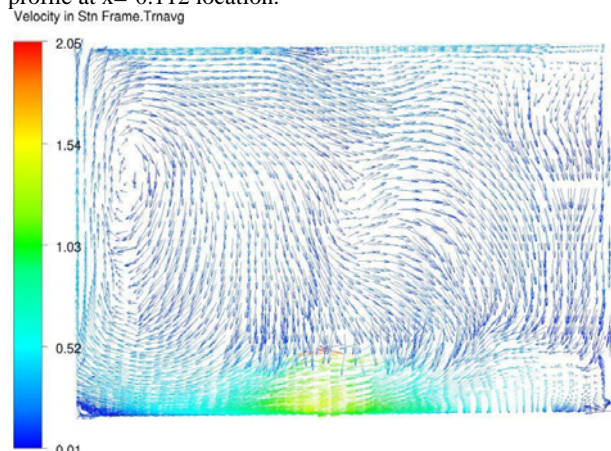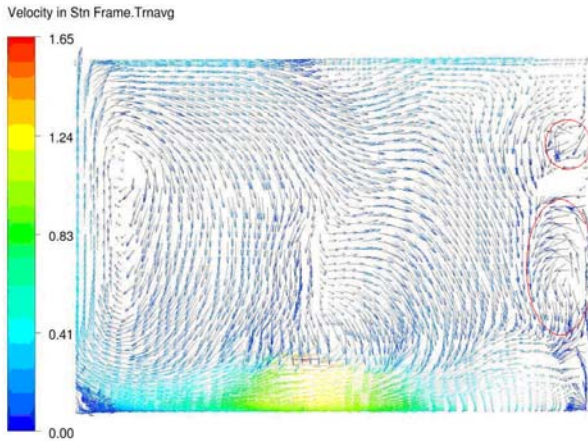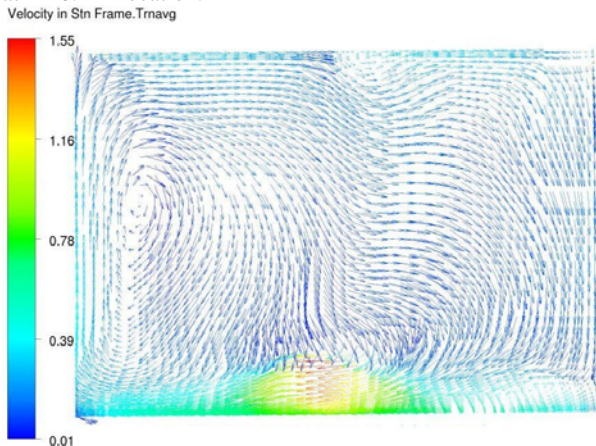

**Figure 6B.** Smagorinsky LES predicted time averaged profile at x=-0.112 location.

Figure 6C. Dynamic LES predicted time averaged profile at x=-0.112 location.

Figure 6D. RANS Model predicted time averaged profile at x=-0.112 location.

Figure 6: Comparison of averaged flow profile captured by various turbulence models and PIV.

The Dynamic LES Model (Fig. 6C), on the other hand, deviates a bit from experimental observation by showing two recirculation's of flow near the right wall (marked in red circles),while the RANS Model (Fig. 6D) shows one circulation covering the whole right side of impeller, here the recirculating flow reaches the right side wall.
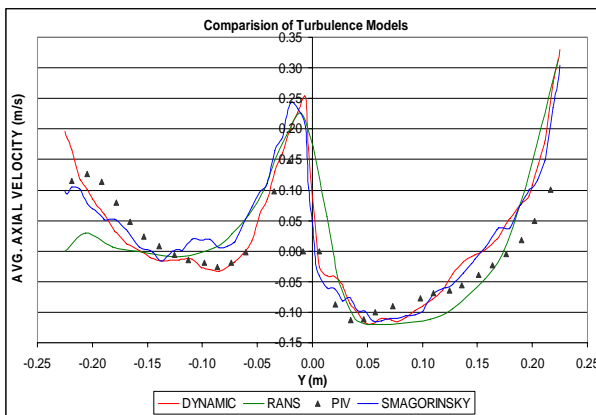

Figure 7: Comparison of Turbulence Models

Fig. 7 compares predicted values to experimental values of time averaged axial velocity along the y direction at location x= -0.168, z = 0.323 for the pump-mixer operating in single phase. Fig. 7 reveals that most computational models deviate from the experiment at y=0,

where they predict a higher positive axial velocity arising from a circulation. Apart from that at other regions, the prediction is within fair agreement. The over-prediction of centre velocity could be a result of higher local values of C_S computed by Germano Model. This could be because the present LES model is moderately resolved.

Flow Pattern

Fig. 8 compares the mean flow profile obtained from the RANS model at a given time (Fig. 8A) with the instantaneous flow profile from Smagorinsky LES (in Fig. 8B). RANS model results are limited to giving information on averaged profiles, while at the same plane, the instantaneous LES (Fig. 8B) is able to capture flow structures (marked in red in Fig. 8). The LES is able to capture precession vortices near the rotating shaft.
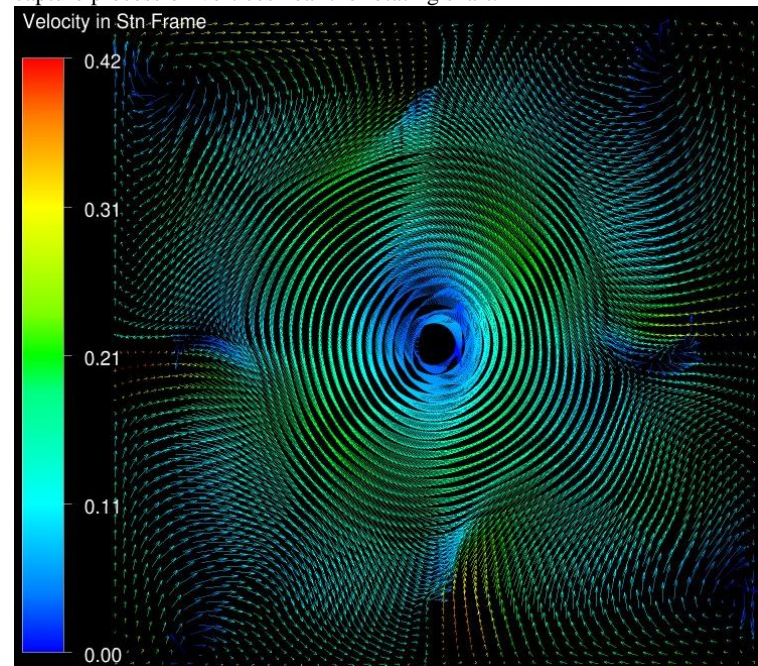
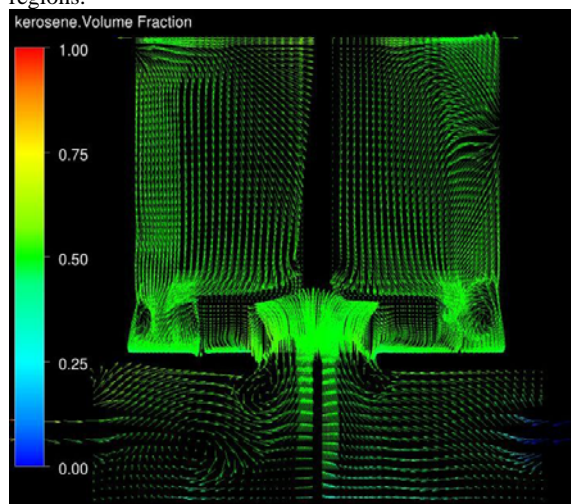**8A.** RANS Model Prediction of Mean Velocity at XY Plane at z=0.42 height.
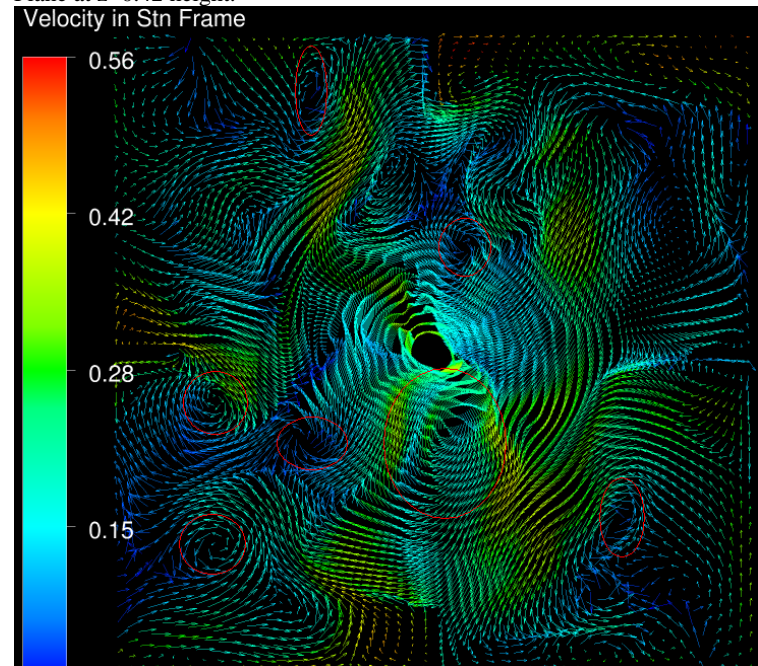
**8B.** LES prediction of Instantaneous Flow at XY Plane at z=0.42 height.

Figure 8: Comparison of flow profiles by RANS and LES
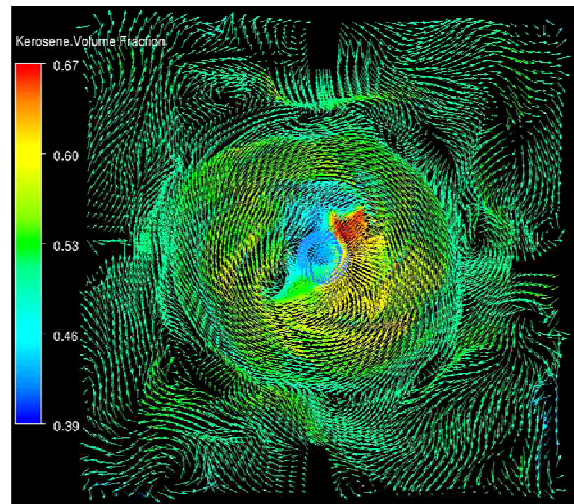
Instantaneous Profiles for Multi-phase Mixer

Fig. 9A shows the velocity profile obtained at a time step by the multiphase RANS model. The RANS model shows only a gross circulation pattern and has not been able to resolve the detailed flow structures. Fig. 9B and 9C shows the instantaneous two phase hydrodynamics captured by Smagorinsky LES, with organic kerosene phase entering the lower left and aqueous phase at lower right of false bottom. Both phases get drawn up by the pump mixer, and dispersion of organic droplet phase and extraction happens in tank. The organic volume fraction is around 50-60% in the tank, where it exists in fine droplet form after being sheared by the impeller. The LES models used have been able to capture the instantaneous flow structures (as marked in red in Fig. 9B). But, these models (Dynamic and Smagorinsky) cannot give the information on sub-grid scale energies, which can be helpful in determining accurately the turbulent dispersion and obtaining accurate total kinetic energy. Hence, the future work would involve obtaining more information using advanced LES models, like one-equation SGS turbulent kinetic energy LES model. The information obtained from this would be useful in understanding effect of turbulence on droplet diameter and mass transfer rates at different regions.

Figure 9A RANS Model Prediction of Mean Velocity and Dispersion in Multiphase system at x=0 location.
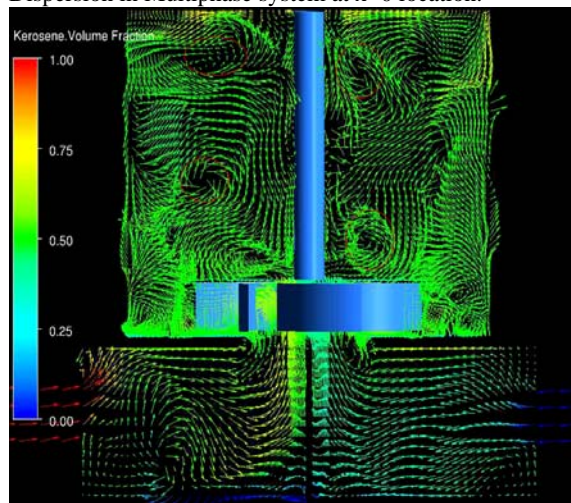
Figure 9B LES based Instantaneous Flow structures and dispersion in Multiphase operation at x=0 location.

Figure 9C LES based Instantaneous Flow structures in Multiphase Operation at Impeller at XY Plane z=0.185 location.

Figure 9: Comparison of flow profiles by RANS and LES

CONCLUSION

The Large Eddy Simulation model has been able to capture the instantaneous flow structures in both single and multiphase operation of the R320 pump mixer. It is expected that more advanced LES models (like one-equation SGS KE) can perhaps show promise for predicting optimum conditions, as they can give information on SGS Kinetic energy and Total Kinetic energy.

ACKNOWLEDGEMENTS

REFERENCES

BAGGETT, J.S., JIMÉNEZ, J., AND KRAVCHENKO, A.G., (1997), "Resolution requirements in large-eddy simulations of shear flows*", Annual Research Briefs*., Stanford Centre for Turbulence Research.

DEEN N., SOLBERG T. and HJERTAGER B., (2001), "Large eddy simulation of gas-liquid flow in a square cross-sectioned bubble column", *Chemical Engineering Science*, **56**, 6341-6349.

DERKSEN, J. J., (2006), "Long-time Solids Suspension Simulations by Means of a Large-Eddy Approach, *Chemical Engineering Research and Design*, **84**, 38.

DERKSEN, J., KONTOMARIS, K., MCLAUGHLIN, J., VAN DEN AKKER, H.E.A., (2007), "Large- eddy simulation of single-phase flow dynamics and mixing in an industrial crystallizer", *Chemical Engineering Research & Design*, **85**, 169–179.

DHOTRE, M.T., NICENO, B. and SMITH, B.L., (2008), "Large eddy simulation of a bubble column using dynamic sub-grid scale model", *Chemical Engineering Journal*, 136(2-3), 337-348.

GERMANO, M., PIOMELLI, U., MOIN, P. AND CABOT, W. H., (1991), "A dynamic subgrid-scale eddy viscosity model", *Physics of Fluids*, **A7,** 1760-1765

HARTMANN, H., DERKSEN, J. AND VAN DEN AKKER, H.E.A., (2006), "Numerical simulation of a dissolution process in a stirred tank reactor", *Chemical Engineering Science*, **61**, 3025.

ISHII M. AND ZUBER N. (1979), "Drag coefficient and relative velocity in bubbly, droplet or particulate flows", *A.I.Ch.E. Journal*, 25, 843-855.

LANE, G., (2006), ˝Flow instability in an alumina precipitator fitted with A draft tube circulator", *Fifth international conference on CFD in the process industries CSIRO, Melbourne, Australia 13-15 December.*

LILLY, D.K., (1992), "A proposed modification of the Germano subgrid-scale closure method", *Physics of Fluids*, **A4**, 633-635.

MOIN, P. AND KIM, J., (1982),"Numerical investigation of turbulent channel flow", *J. Fluid Mech.,* 118, 341–377.

MURTHY, B.N. and JOSHI, J.B., (2008), "Assessment of standard $k-\varepsilon$, RSM and LES turbulence models in a baffled stirred vessel agitated by various impeller designs", *Chemical Engineering Science*, **63**, 5468 -5495.

NICENO, B., DHOTRE, M.T. and SMITH, B.L. (2008), "One-equation sub-grid scale (SGS) modelling for Euler-Euler Large Eddy Simulation (EELES) of dispersed bubbly flow", *Chemical Engineering Science,* **63**, 3923 - 3931.

POPE, S.B., *Turbulent Flows*. 2000: Cambridge University Press. 12.

SMAGORINSKY, J., (1963),"General circulation experiments with the primitive equations: 1. The basic experiment", *Monthly Weather Review*, 99-164.

TABIB M.V., ROY S.A. AND JOSHI, J.B., (2008), "CFD simulation of bubble column—an analysis of interphase forces and turbulence models", *Chemical Engineering Journal,* **139,** 589–614.